Prediction of restriction in output current by reactant flow in redox flow battery for compensating load variations

Toko Mannari, Takafumi Okuda, and Takashi Hikihara
Kyoto University

October 22, 2020

Abstract

Redox flow batteries (RFBs) connected to the power grid can absorb load variations which appear in several time scales. An RFB consists of a cell stack as the chemical-reaction element and tanks as the storage element. An electrolytes are pumped and circulated between them. The cell stack can supply power as long as reactants are supplied to the stack. The slow velocity of the reactant flow to the cells restricts the output current, and the RFB can not supply the requested power under the current restriction. The reactant flow should be considered for confirming whether the RFB can supply the requested power at load variations. This paper proposes the method to predict the current restriction by the reactant flow through simulations. The method is based on a chemical reaction model. The model enables us to simulate the time evolution of the reactant concentration, which governs the electrical behavior and the reactant flow of the RFB. The current available from the reactant flow is introduced to estimate the current restriction by the slow velocity of the reactant flow. The proposed method predicts well the current restriction of the prototype RFB, which is integrated into a 300 A class discharging circuit.

1 Introduction

The energy storage systems have been installed to the power grid for compensating the load variations found in several time scales. The energy storage systems are required to have the wide capabilities adjusting to the time scale of the load variations [1]. The large energy capacity is required to level the load variation in the scale of hours, and the quick response is necessary for smoothing the fluctuations in the scale of second or minute. The energy storage in the uninterruptible power supply (UPS) is designed to output high power instantly for maintaining power quality. Few energy storage systems satisfy these all requirements.

Redox flow battery (RFB) [2] is one of the energy storage systems which can satisfy the requirements. The RFB is a secondary battery which is equipped with the circulation

system of the electrolytes. The RFB consists of two components called "cell stack" and "tank." Each cell in the stack converts the chemical energy to the electrical energy through the oxidation-reduction (redox) reaction. The tanks store the electrolytes. The electrolytes circulate between the cell stack and the tanks. The circulation system of the electrolyte carries the reactants to the cells for keeping the redox reaction in the cell. The energy capacity depends on the volume of the tanks, and the output capacity is determined by the number of the cells. The energy capacity and the output capacity are easily enlarged by increasing the number of the cells and the volume of the tanks [3, 4]. Furthermore, the RFB can respond to the load variation in milliseconds [5, 6]. The RFB system of 6 MWh has demonstrated to the load-leveling and the smoothing output power of the wind farm [7]. The UPS with the RFB was also installed at some data centers for compensating the voltage sag [8].

The reactant flow obviously governs the characteristics of the RFBs, when is keeping the power supply at the large change of the load current. The reactants in the cells are rapidly consumed due to the sudden increase of the current. The slow velocity of the reactants' flow leads running out of the reactants in the cell. Then, the voltage drops, and the current appears the restriction due to the reactant flow. As a result, the RFB cannot supply the requested power to the load under the restriction. The current restriction should be avoided.

If the current restriction can be predicted in the simulation, the simulation result gives the direction to construct the system for avoiding the current restriction. The circuit can be designed with consideration for the ability of the RFB as the power supply, which is evaluated through the simulation. Moreover, the current restriction can be avoided by controlling the current or the electrolyte flow based on the prediction.

We easily find simulations for confirming the performance of the circuit, with the electrochemical devices, including the battery and the fuel cell (FC) [9, 10, 11]. The electrochemical devices are regarded as the constant voltage sources for simulating the electrical behavior of them in the scale of millisecond or microsecond [9, 10]. The electrical behavior of the electrochemical device, however, is affected by the mass transfer and the reaction in the scale of second. The phenomena cannot be neglected in continuous operation, which is longer than seconds. Paja *et. al.* [11] took the reactant flow into account for predicting the FC's electrical behavior in the scale of second. The electrical behavior of the RFB is also required to be simulated with the consideration for the reactant flow as well as the FC in the research [11].

The models [12, 13, 14] enable us to simulate the discharging behavior of the RFB with the consideration for the reactant flow. These models describe the dynamics in the reactant concentration based on chemical kinetics and mass transport. Especially, the model with transport delay [12] is considering the finite transport time from the tanks to the cell, while the models in the papers [13, 14] are neglecting the transport time. The reactant flow from the tank to the cell stack is slow with comparison to the current in the electrical circuit. The reactants in the tanks take a finite time to move to the cell stack. The transport time becomes critical for predicting the restriction by the reactant flow from the tanks to the cell stack. The model with transport delay [12] is suitable for

the prediction in the time duration.

In addition to the model for simulation, the indicator is needed for detecting the current restriction. The researches [15, 16] employ the SOC of the cells as the simplest indicator. The amount of the reactants is reflected on the SOC, which can be easily estimated by adding the monitor cell to the circulation system of the electrolyte[17, 18]. The control strategies [15, 16] set the limitation on the SOC and control the current within the limitation of SOC. However, the condition for the current restriction differs depending on the current and velocity of the reactant flow. The use of SOC is not enough to grasp the current restriction completely.

The current determined by the rate of mass transfer is employed as the indicator referring to current restriction in the charging behavior [20, 21]. The current coincides with the value obtained from the rate of mass transfer when the mass transfer restricts the current [19]. The control strategy proposed by Akter *et. al.*[20, 21] employs the current determined by the rate of diffusion to detect the current restriction by diffusion inside of the cell. The rate of diffusion is given by the function of reactant concentration, length of diffusion layer, and diffusion coefficient. The parameters related to the diffusion are affected by the flow rate of the electrolyte and the SOC. It is impossible to verify these variables in operation. We focus on the reactant flow from the tanks to the cells as an alternative to the diffusion inside of the cell. The velocity of the reactant flow is determined by the flow rate of the electrolyte and the reactant concentration. The flow rate of the electrolyte is observable, and the reactant concentration can be estimated from the EMF of the cells. The current determined by the reactant flow from the tanks to the cell is called "limited-current" in this paper. The limited-current is applied for clarifying the current restriction at the discharge.

This paper proposes the method to predict the current restriction by the reactant flow of the RFB. The reactant concentration and the electrical behavior are simulated by the model with transport delay [12]. The restriction is detected from the convergence of the current to the limited-current. Section 2 introduces the limited-current and the model as the tool for predicting current restriction. The tools are applied to predict the current restriction of the RFB in section 3. The RFB is connected to the load resistances and discharges under the load variations. The result is verified in the experiment with the 300 A class discharging circuit in section 4. It verifies that the current in the experiment behaves similarly to the proposed method.

2 Tool for predicting current restriction by reactant flow

2.1 Charging/discharging mechanism of cell

This subsection explains the charging/discharging mechanism of a cell. The scheme of the reaction system in the cell is described in Figure 1. The following redox reaction (1)

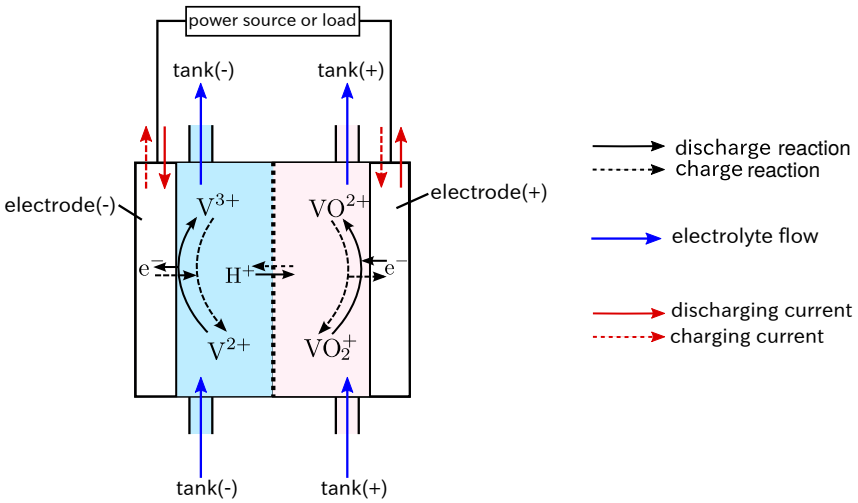

Figure 1: Charging/discharging mechanism of cell. The reactants V^{2+} and VO_2^+ are consumed by the discharging reaction. The electrolyte flow supplies the reactants from the tanks to the cell. The charging/discharging of the cell is defined as the increase/decrease of the reactant concentration in the cell.

occurs in the cell, connected to a load or a power source.

$$\begin{cases} V^{2+} \rightleftharpoons V^{3+} + e^- & (\text{Negative electrode}) \\ VO_2^+ + 2H^+ + e^- \rightleftharpoons H_2O + VO^{2+} & (\text{Positive electrode}) \end{cases} \tag{1}$$

The forward reaction and reverse reactions correspond to discharging and charging reaction respectively. For discharging, V^{2+}, $VO_2{}^+$, and H^+ are the reactants. Protons transfer between the negative and positive half cells accompanies redox reaction (1).

$$H^+(\text{Negative half cell}) \rightleftharpoons H^+(\text{Positive half cell}) \tag{2}$$

The EMF of the cell is given by Nernst equation [22] (3).

$$E_e = E_{eo} + \frac{RT}{F} \ln \frac{[V^{2+}][VO_2^+][H^+]^2}{[V^{3+}][VO^{2+}]} \tag{3}$$

The variation in $[H^+]$ is negligible in the EMF [23]. Equation (3) is simplified by assuming that the reactions in the positive and negative half cells keep the symmetry.

$$\begin{aligned} E_e &= E_{eh}^0 + \frac{2RT}{F} \ln \frac{c}{c_{max} - c} \\ &= E_{eh}^0 + \frac{2RT}{F} \ln \frac{[V^{2+}]}{c_{max} - [V^{2+}]} = E_{eh}^0 + \frac{2RT}{F} \ln \frac{[VO_2^+]}{c_{max} - [VO_2^+]} \end{aligned} \tag{4}$$

Here, $c = [V^{2+}] = [VO_2^+]$ and $c \in (0, c_{max})$ [24]. E_{eh}^0 is the EMF at $c = c_{max}/2$.

The following explanation also holds the symmetry between the positive and negative half cells and refers $c = [V^{2+}] = [VO_2^+]$ as the reactant concentration. In equation (4), the EMF monotonically increases with the reactant concentration c. The charging/discharging of the cell is defined as the increase/decrease of the reactant concentration in the cell. The cell can output the electric power as long as the reactants are supplied to the cell.

2.2 Limited-current determined by reactant flow

This subsection introduces the limited-current, which indicates the restriction of the current by the reactant flow. The limited-current is introduced based on the reaction process in the negative half cell.

Let $v_{\mathrm{r}-}$ be the rate of discharging reaction in the negative half cell. Faraday's law of electrolysis [19] gives the following relationship between the rate of discharging reaction $v_{\mathrm{r}-}$ and the discharging current.

$$I(t) = \alpha_{\mathrm{c}} F v_{\mathrm{r}-} \tag{5}$$

The following equation (6) gives the rate of V^{+} flowing into the negative half cell.

$$v_{\mathrm{f}-}(t) = \frac{W_{\mathrm{c}}}{\alpha_{\mathrm{c}}} [\mathrm{V}^{2+}]_{\mathrm{t}}(t - \tau_{\mathrm{d}}) \tag{6}$$

The transport time from the tanks to the cell is taken into account here, and $[\mathrm{V}^{2+}]_{\mathrm{t}}(t-\tau_{\mathrm{d}})$ represents the concentration of V^{2+} in the negative tank at $t = t - \tau_{\mathrm{d}}$. W_{c} is the flow rate of the electrolyte, and α_{c} is the volume of the electrolyte in the negative half cell.

Suppose that most of V^{+} in the negative half cell is consumed due to the high current and a-1111 fast discharging reaction. The rate of the discharging reaction $v_{\mathrm{r}-}$ is restricted by the flow of reactant $v_{\mathrm{f}-}$ following equation (7).

$$v_{\mathrm{r}-}(t) = v_{\mathrm{f}-}(t) \tag{7}$$

The limited-current I_{lim} is given by the combination of equations (5)–(7).

$$I_{\mathrm{lim}}(t) = F W_{\mathrm{c}} [\mathrm{V}^{2+}]_{\mathrm{t}}(t - \tau_{\mathrm{d}}) \tag{8}$$

The limited-current can also be introduced from the discharging reaction in the positive half cell by proceeding along with the introduction from the negative half cell. The limited-current can be rewritten to the following equation (9) from the symmetry between the negative and the positive half cell.

$$I_{\mathrm{lim}}(t) = F W_{\mathrm{c}} c_{\mathrm{tank}}(t - \tau_{\mathrm{d}}) \tag{9}$$

$c_{\mathrm{tank}}(t)$ is the reactant concentration in the tank. The current is restricted by the limited-current I_{lim} when the reactant flow restricts the discharging reaction.

2.3 Model for simulating reactant concentrations

Here is applied the model of charging/discharging dynamics with transport delay [12] for simulating the time evolution of the reactant concentration, the voltages, and the current. The model is explained as follows.

The target system of the model is described in Figure 2. The cell stack of the RFB consists of 10 main cells and 1 monitor cell. The main cells are electrically connected in series. V_{main} is the total voltage of the main cells. The port of the monitor cell is opened.

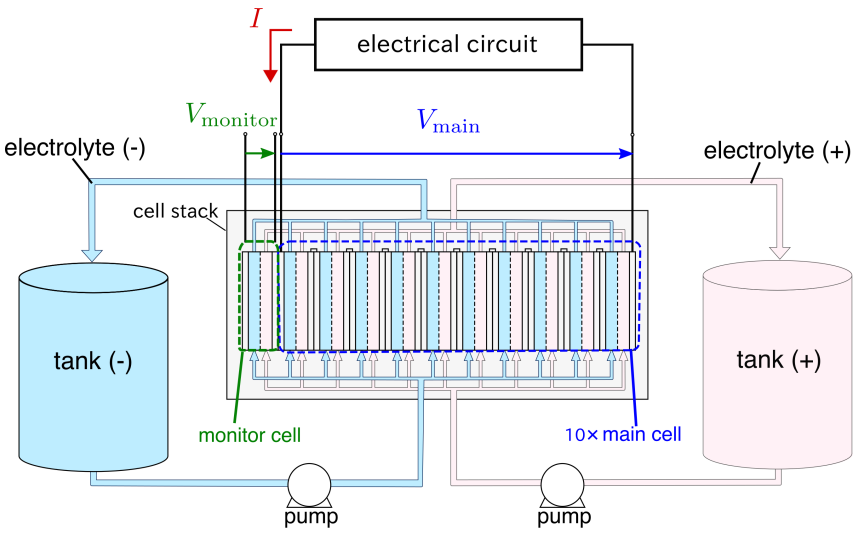

Figure 2: RFB as target system of modeling. The RFB consists of a cell stack and tanks. The cell stack is composed of 10 main cells and 1 monitor cell. The main cells are connected in series. The port of the monitor cell is opened. The electrolytes flow through these cells in parallel. V_{main} is the total voltage of the main cells. V_{monitor} is the voltage of the monitor cell, which shows the electromotive force. I is the current.

V_{monitor} represents the EMF of the monitor cell. The electrolytes flow into the cells in parallel.

$V_{\mathrm{main}}(t)$ and $V_{\mathrm{monitor}}(t)$ hold the following equation (10) from equation (4).

$$\begin{cases} V_{\mathrm{main}}(t) & = m\left(E^0_{\mathrm{eh}} + \dfrac{2RT}{F}\ln\dfrac{c_{\mathrm{main}}(t)}{c_{\max} - c_{\mathrm{main}}(t)} - r_{\mathrm{rfb}}I\right) \\ V_{\mathrm{monitor}}(t) & = E^0_{\mathrm{eh}} + \dfrac{2RT}{F}\ln\dfrac{c_{\mathrm{monitor}}(t)}{c_{\max} - c_{\mathrm{monitor}}(t)} \end{cases} \tag{10}$$

Where, $m = 10$ as the number of main cells. c_i $(i = \text{main and monitor})$ is the reactant concentration in the cell. $r_{\mathrm{rfb}}I$ represents the loss, including the ohmic loss and the overpotentials [19].

The following delay differential equations (DDEs) (11) and (12) give the time evolution of the reactant concentration in the cells [12].

$$\begin{aligned} \frac{\mathrm{d}^2 c_{\mathrm{main}}(t)}{\mathrm{d}t^2} = &-\frac{W_{\mathrm{c}}}{\alpha_{\mathrm{c}}}\frac{\mathrm{d}c_{\mathrm{main}}(t)}{\mathrm{d}t} - \frac{mW_{\mathrm{c}}}{\alpha_{\mathrm{t}}}\frac{\mathrm{d}c_{\mathrm{main}}(t-\tau_{\mathrm{d}})}{\mathrm{d}t} - \frac{W_{\mathrm{c}}}{\alpha_{\mathrm{t}}}\frac{\mathrm{d}c_{\mathrm{monitor}}(t-\tau_{\mathrm{d}})}{\mathrm{d}t} \\ &- \frac{mW_{\mathrm{c}}I(t-\tau_{\mathrm{d}})}{\alpha_{\mathrm{c}}\alpha_{\mathrm{t}}F} - \frac{1}{\alpha_{\mathrm{c}}F}\frac{\mathrm{d}I(t)}{\mathrm{d}t} \end{aligned} \tag{11}$$

$$\begin{aligned} \frac{\mathrm{d}^2 c_{\mathrm{monitor}}(t)}{\mathrm{d}t^2} = &-\frac{W_{\mathrm{c}}}{\alpha_{\mathrm{c}}}\frac{\mathrm{d}c_{\mathrm{monitor}}(t)}{\mathrm{d}t} - \frac{mW_{\mathrm{c}}}{\alpha_{\mathrm{t}}}\frac{\mathrm{d}c_{\mathrm{main}}(t-\tau_{\mathrm{d}})}{\mathrm{d}t} - \frac{W_{\mathrm{c}}}{\alpha_{\mathrm{t}}}\frac{\mathrm{d}c_{\mathrm{monitor}}(t-\tau_{\mathrm{d}})}{\mathrm{d}t} - \\ &- \frac{mW_{\mathrm{c}}I(t-\tau_{\mathrm{d}})}{\alpha_{\mathrm{c}}\alpha_{\mathrm{t}}F} \end{aligned} \tag{12}$$

α_t is the volume of the electrolyte in the tank. $dI(t)/dt$ in DDE (11) reflects the dynamics of the electrical circuit. The DDEs (11) and (12) are introduced from the mass balance equations [25] in the cells and the RFB under the following assumptions.

(a1) The reactants distribute uniformly in the cells and the tanks.

(a2) The time τ_d is required to transport the reactants in the tanks to the cell stack.

(a3) The ions cannot go across the membrane except for H^+.

The discharging current can be simulated by coupling the equations (10)–(12) with the equations for the electrical circuit.

The reactant concentration in the negative tank $c_{tank}(t)$ is needed for calculating the limited-current I_{lim}. The $c_{tank}(t)$ is given by solving the differential equation of $c_{tank}(t)$, which is introduced from the following mass balance equation (13) in the RFB.

$$N(t) = m\alpha_c c_{main}(t) + \alpha_c c_{monitor}(t) + \alpha_t c_{tank}(t) \tag{13}$$

$N(t)$ is the total molar amount of V^{2+} or $VO_2{}^+$ in the RFB. The differential equation of $c_{tank}(t)$ is given by differentiating the mass balance equation (13).

$$\frac{dc_{tank}(t)}{dt} = \frac{1}{\alpha_t}\left(-\frac{mI(t)}{F} - m\alpha_c\frac{dc_{main}(t)}{dt} - \alpha_c\frac{dc_{monitor}(t)}{dt}\right) \tag{14}$$

I_{lim} is calculated by substituting the solution of the differential equation (14) to equation (9).

3 Prediction of restriction in current by reactant flow in discharging circuit

The RFB described in Figure 2 is integrated into a 300 A class discharging circuit in this section. The restriction by the reactant flow is predicted by the model and the indicator.

3.1 Setting for discharging circuit and load variation

Suppose that the RFB is integrated into the discharging circuit described in Figure 3. L denotes a parasitic inductance. Every load resistance, r_{load}, is connected to a MOSFET in series. The load of the RFB is discontinuously changed by switching with the MOSFETs. The MOSFETs are assumed to switch instantly.

Kirchhoff's voltage law gives the current change in the discharging circuit by equation (15).

$$\frac{dI(t)}{dt} = -\frac{1}{L}\left\{\left(\frac{r_{load}}{n(t)}\right)I(t) - V_{main}(t)\right\} \tag{15}$$

n denotes the number of load resistances connected to the RFB.

The number of connected resistances, n, changes under the following two modes.

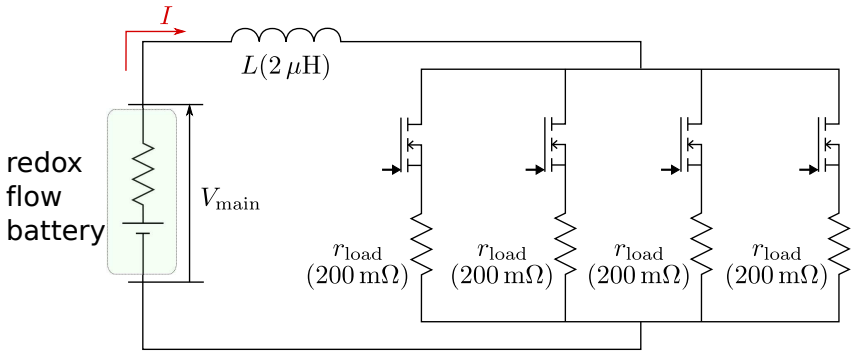

Figure 3: Discharging circuit integrating an RFB. Every load resistance, r_{load}, is connected to a MOSFET in series. The number of loads connected to the RFB changes by MOSFET switching, which represents the load variation. I is the discharging current, and V_{main} is to total voltage of the main cells.

1. Constant load mode;

$$n(t) = 4,\ t \geq 0 \tag{16}$$

2. Periodic load variation mode;

$$n(t) = \begin{cases} 4 & \left(k\Delta t \leq t < \dfrac{2k+1}{2}\Delta t\right) \\ 1 & \left(\dfrac{2k+1}{2}\Delta t \leq t < (k+1)\Delta t\right) \end{cases} \tag{17}$$

Here, $k \in \mathbb{Z}$, $k \geq 0$, and Δt is the period of load variation.

3.2 Simulation results

This subsection simulates the discharging behavior of the RFB in the discharging circuit using the RFB parameters listed in table 1.

Table 1: Parameter setting for model of RFB.

Symbol	Name	Value
m	Number of cells	10
W_{c}	Flow rate of electrolyte per cell	$0.6\,\text{L}\,\text{min}^{-1}$
α_{t}	Volume of electrolyte per tank	7.31 L
α_{c}	Volume of electrolyte per cell	40 m L
r_{rfb}	Internal resistance per cell	$2.1\,\text{m}\,\Omega$
T	Temperature	305K
τ_{d}	Transport delay	19s

The discharging behavior is simulated by solving differential equations (11), (12), (14), and (15) for the following initial condition (18).

$$\begin{cases} c_{\mathrm{main}}(t_0) & = c_{\mathrm{monitor}}(t_0) = c_{\mathrm{tank}}(t_0) = 0.8\,\mathrm{mol L^{-1}}, \\ \dfrac{\mathrm{d}c_{\mathrm{main}}(t_0)}{\mathrm{d}t} & = \dfrac{\mathrm{d}c_{\mathrm{monitor}}(t_0)}{\mathrm{d}t} = \dfrac{\mathrm{d}c_{\mathrm{tank}}(t_0)}{\mathrm{d}t} = 0, \\ I(t_0) & = 0 \end{cases} \tag{18}$$

Here, $-\tau_{\mathrm{d}} \leq t_0 \leq 0$. The fourth order Runge–Kutta method [26, 27] was applied for the simulation. The step size is fixed at 10^{-5} s. The reactant concentration should be positive, and the finishing condition is given as follows.

$$(c_{\mathrm{main}}(t) \leq 0) \cup (c_{\mathrm{monitor}}(t) \leq 0) \cup (c_{\mathrm{tank}}(t) \leq 0) \tag{19}$$

The simulation results for constant load mode (16) are shown in Figure 4(a). The discharging behavior after $t = 300$ s indicates the restriction due to reactant flow. The discharging current converges to limited-current and decreases quickly. The order of c_{main} is smaller than $10^{-3}\,\mathrm{mol L^{-1}}$ at this term. The simulation stops around $t = 350$ s after satisfying finishing condition (19).

For the periodic load variation, we set Δt to 120 s. The restriction after the load variation is shown in Figure 4(b). The current behavior is restricted by the limited-current around $t = 400$ s and exceeds the limited-current after switching at $t = 480$ s. The temporary increase of I is considered to be caused by the increase of c_{main}. In fact, a larger amount of V^{2+} flows into the cells than the consumption due to the discharging reaction after switching at $t = 400$ s. Therefore, c_{main} temporally increases, and the condition for the reactant flow to restrict the current is not satisfied in this short period. Then, the replenished reactants are consumed instantly due to the sudden increase of the current at 480 s, and the current is restricted by the reactant flow again.

The rate of discharge $\mathrm{d}c_i/\mathrm{d}t$ can be related to the current restriction. $\mathrm{d}c_i/\mathrm{d}t$ converges to the following value for $I \ll I_{\mathrm{lim}}$ in Figure 5.

$$\frac{\mathrm{d}c_i(t)}{\mathrm{d}t} \to -\frac{mI(t-\tau_{\mathrm{d}})}{((m+1)\alpha_{\mathrm{c}} + \alpha_{\mathrm{t}})F} = f(I(t-\tau_{\mathrm{d}})) \tag{20}$$

If $I \approx I_{\mathrm{lim}}$, $\mathrm{d}c_{\mathrm{main}}/\mathrm{d}t$ does not approach the line corresponding to $f(I(t-\tau_{\mathrm{d}}))$. The rate of discharge $\mathrm{d}c_{\mathrm{main}}/\mathrm{d}t$ reaching 0 can be clearly explained using the following mass balance equation in a main cell.

$$\frac{\mathrm{d}c_{\mathrm{main}}(t)}{\mathrm{d}t} = -\frac{I(t)}{\alpha_{\mathrm{c}}F} + \frac{W_{\mathrm{c}}}{\alpha_{\mathrm{c}}}(c_{\mathrm{tank}}(t-\tau_{\mathrm{d}}) - c_{\mathrm{main}}(t)) \approx 0 \tag{21}$$

Here, the first term corresponds to the reaction, and the other terms represent the inflow and the outflow of reactants. $\mathrm{d}c_{\mathrm{main}}/\mathrm{d}t = 0$ is obtained by substituting $c_{\mathrm{main}}(t) = 0$ and $I = I_{\mathrm{lim}}$ into mass balance equation (21).

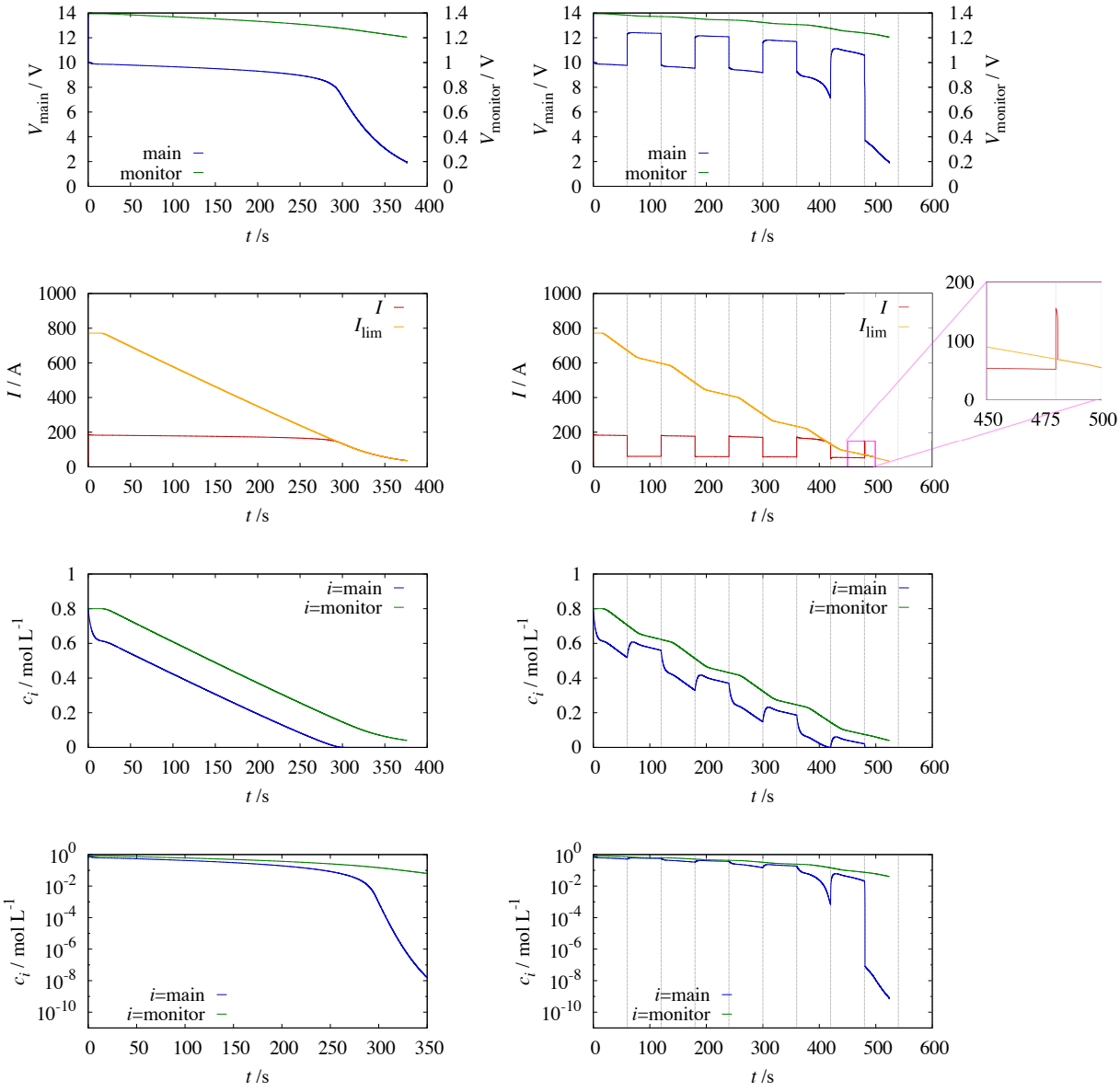

(a) Constant load mode.

(b) Load variation mode.

Figure 4: Simulation results for two load modes. (a) Constant load mode for 4 connected load resistances. (b) Periodic load variation mode, where the number of load resistances, n, changes periodically between 1 and 4. The period is 120 s.

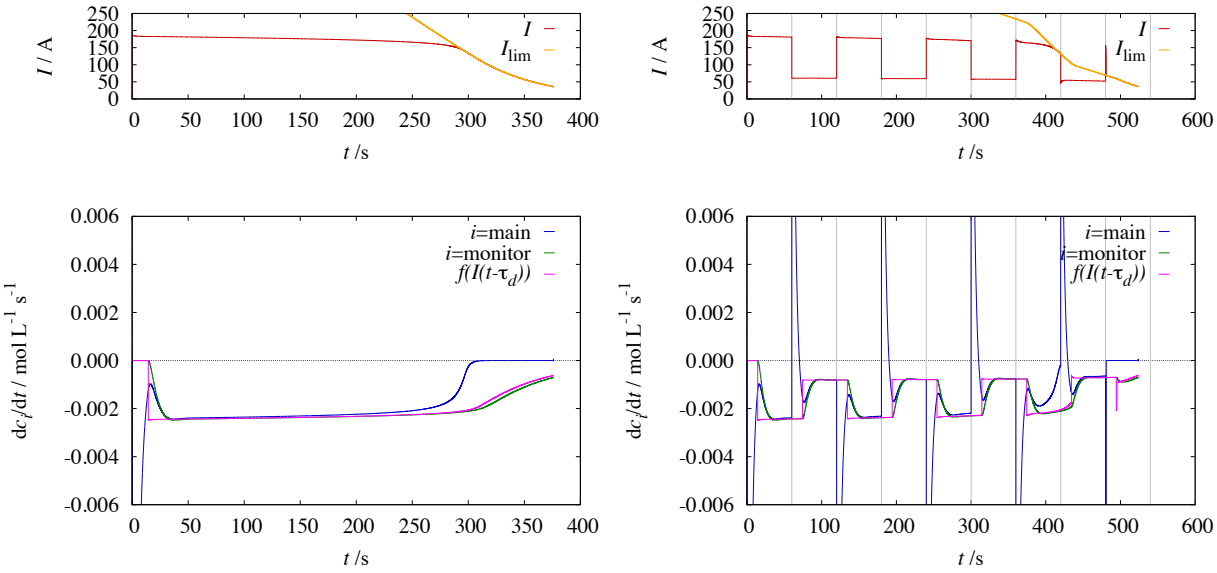

(a) Constant load mode.

(b) Load variation mode.

Figure 5: Rate of discharge $\mathrm{d}c_i/\mathrm{d}t$ for two load modes. The line refers $\mathrm{d}c_i/\mathrm{d}t$ in steady state for $I \ll I_{\mathrm{lim}}$. (a) Constant load mode for 4 connected load resistances. (b) Periodic load variation mode, n, changes periodically between 1 and 4. The period is 120 s.

4 Verification of prediction with experimental system

This verifies whether the current behavior restricted by the reactant flow appear in the experimental system like in the simulation prediction reported in section 3.

4.1 Experimental setup

Figure 6 shows the prototype RFB system and the 300 A class discharging circuit.

The discharging circuit shown in Figure 3 is implemented. The circuit consists of an output port of the prototype RFB, load resistances, Si MOSFETs (IXFN, IXFN420N10T), and additional capacitors of 100 μF. Each capacitor is connected in parallel with a MOSFET for suppressing surge voltages. The rated power of each load resistance (200 mΩ) is 800 W.

Each MOSFET is driven by a gate driver (Silicon Labs, Si8235BB-C-IS1). The input signals to the gate drivers are generated by a controller board (National Instruments, sbRIO 9607). For protection, the output port of the controller is isolated from the input port of the gate driver.

The state of MOSFETs S_j ($j = 1$, 2, 3, and 4) switches according to the load modes.

1. For the constant load mode:

$$S_j = \mathrm{ON},\ j = 1,\ 2,\ 3,\ \text{and}\ 4 \tag{22}$$

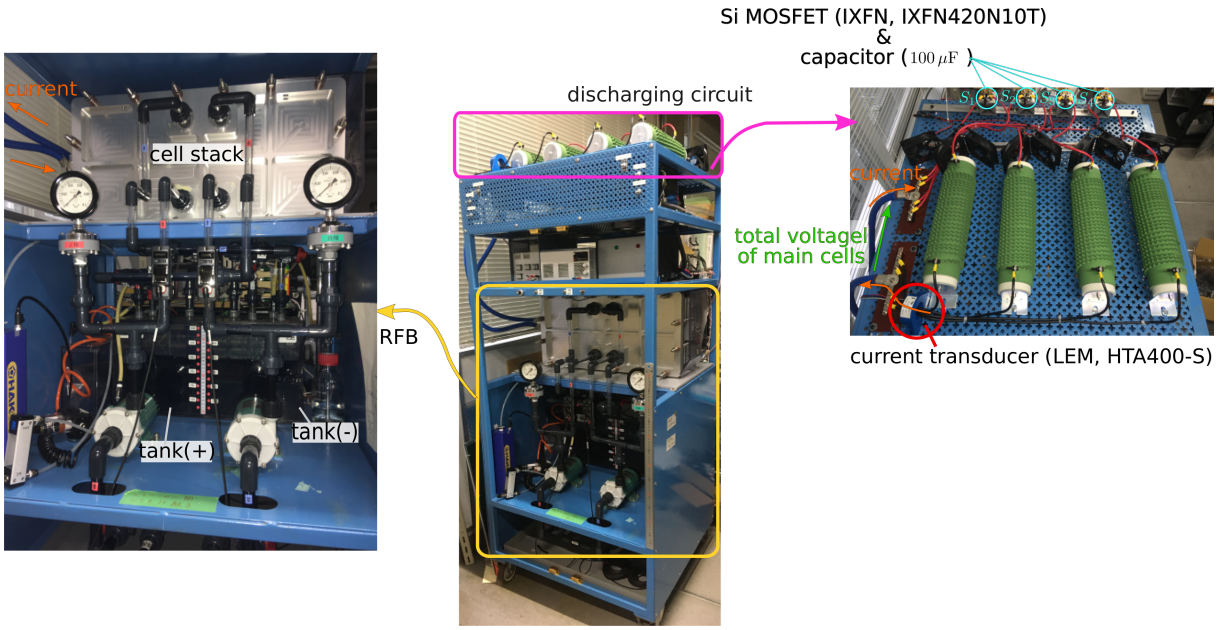

Figure 6: Photograph of experimental setup. This system consists of an prototype RFB and a discharging circuit. The state of MOSFETs S_j ($j = 1$, 2, 3, and 4) changes according to the signal generated by the controller.

2. For the periodic load variation mode:

$$S_1 = S_2 = S_3 = \begin{cases} \text{ON} & \left(k\Delta t \leq t < \dfrac{2k+1}{2}\Delta t\right) \\ \text{OFF} & \left(\dfrac{2k+1}{2}\Delta t < t < (k+1)\Delta t\right) \end{cases} \tag{23}$$

$$S_4 = \text{ON} \ (t \geq 0)$$

The voltages and the current are measured with a current transducer (LEM, HTA 400-S) and a memory hicoder (HIOKI, 4081). The value of the current was converted into a voltage signal with the current transducer. The memory hicoder stores the converted voltage signal, the total voltage of the main cells (V_{main}), and EMF of the monitor cell (V_{monitor}).

4.2 Comparison of simulation to experimental result

This subsection compares the experimental result with the simulation result in subsection 3.2. The reactants were distributed uniformly in the RFB before discharging. The main cells were not connected to the discharging circuit in $t < 0$, and all MOSFETs were activated at $t = 0$.

The experimental result is compared to the simulation result in Figure 7. The prototype RFB shows similar behaviors to the simulation results. The current drops rapidly around $t = 300\,\text{s}$ in the constant load mode, as shown in Figure 7(a). In addition, Figure

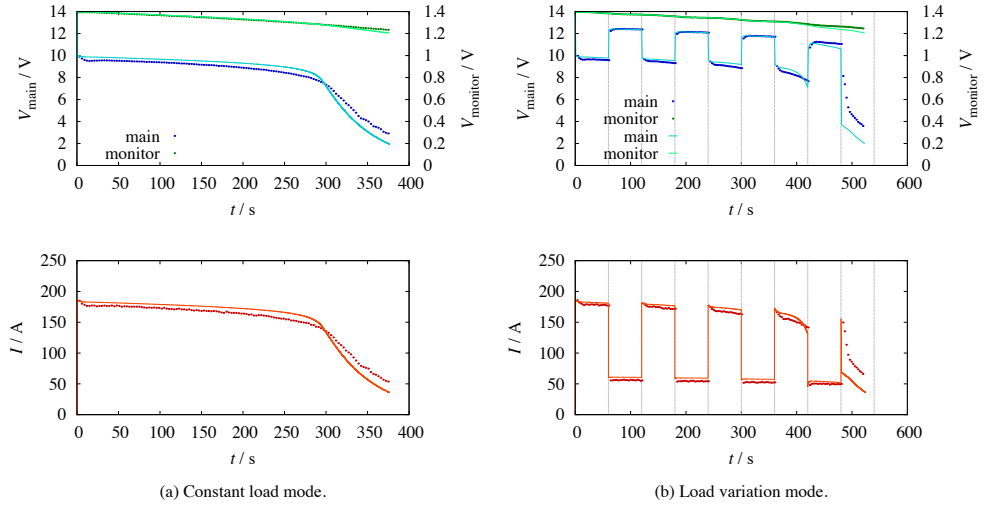

(a) Constant load mode.

(b) Load variation mode.

Figure 7: Comparison between experimental and simulation results. The dotted lines indicate the experimental results, and the solid lines indicate the simulation results. (a) Constant load mode for 4 connected load resistances. (b) Periodic load variation mode, where the number of load resistances, n, changes periodically between 1 and 4. The period is 120 s.

7(b) shows that the current is restricted after the temporary increase of the current in the prototype, being consistent with the simulation.

Figure 7 also shows that the prototype RFB has a slower discharge when compared with the simulation before the current restriction. The rate of discharge is determined by the load current according to equation (20). The current measured in the experiment is smaller than that in the simulation. The RFB in the experiment represents a slower discharge than the simulation due to this smaller current.

The difference in the experimental and simulation currents indicates the occurrence of concentration overpotential [19]. Concentration overpotential degrades the output current depending on the gradient of the reactant concentration along the vertical direction to the electrode. The internal resistance increases with concentration overpotential. The concentration overpotential has been discussed in high power RFB systems [28]. The model in subsection 2.3 assumes the constant internal resistance. The current in the simulation coincides with the experiment at $t = 0$ in Figure 4(a) and at switching from n of 1 to 4 in Figure 4(b). The resistance listed in table 1 is valid at these instants. However, the current changes transiently, and the value in the experiment becomes smaller than the simulation. The transient behavior appears by the high current. The transient behavior may be derived from concentration overpotential.

The purpose of predicting the restriction is to examine the ability of the RFB to maintain the power supply under load variation. The concentration overpotential is not critical during the variation. The prototype RFB discharges more slowly with comparison to the simulation. The reactant flow does not restrict the current in the experimental system if the model is not restricted in the same term.

5 Conclusion

The prediction method proposed in this paper enables us to confirm whether the RFB can supply the requested power under load variations. The current restricted by the reactant flow is simulated by the model with transport delay, and the limited-current works as the indicator of the current restriction. The current in an experimental system is restricted by the reactant flow, as predicted in the simulation. The current restriction in the experiments appears after than in the simulation because of the fast rate of discharge. The ability of the RFB as the power supply is secured in the time domain, in which the RFB in the simulation discharges without the restriction. The difference in the rate of discharge is not critical for confirming the ability of the RFB in the circuit under the load variations. The circuit integrating the RFB can be designed based on the confirmitation.

The proposed prediction method also has a potential to contribute to avoid the current restriction by the reactant flow. The reactant flow depends on the flow rate of the electrolyte. The current restriction can be avoided by controlling the electrolyte flow based on the prediction of the current restriction if the accuracy of the prediction is improved.

Acknowledgments

This research was supported by JSPS KAKENHI grant number JP19J11075, Super Cluster Program from Japan Science and Technology Agency. And the prototype RFB system is provided by Sumitomo Electric Industries, Ltd.

References

[1] Molina MG. Energy Storage and Power Electronics Technologies: A Strong Combination to Empower the Transformation to the Smart Grid. *Proceedings of the IEEE* 2017; 105(11): 2191–2219. doi: 10.1109/JPROC.2017.2702627

[2] Skyllas-Kazacos M, Rychcik M, Robins RG, Fane AG, Green MA. New All-Vanadium Redox Flow Cell. *Journal of The Electrochemical Society* 1986; 133(5): 1057–1058.

[3] Nguyen TA, Crow ML, Elmore AC. Optimal Sizing of a Vanadium Redox Battery System for Microgrid Systems. *IEEE Transactions on Sustainable Energy* 2015; 6(3): 729–737. doi: 10.1109/TSTE.2015.2404780

[4] Poullikkas A. A comparative overview of large-scale battery systems for electricity storage. *Renewable and Sustainable Energy Reviews* 2013; 27: 778–788.

[5] Kaizuka T. Evaluation of Control Maintaining Electric Power Quality by use of Rechargeable Battery System. *2001 IEEE Power Engineering Society Winter Meeting. Conference Proceedings* 2000;1;88–93.

[6] Li Y, Bao J, Skyllas-Kazacos M, Akter MP, Zhang X, Fletcher J. Studies on dynamic responses and impedance of the vanadium redox flow battery. *Applied Energy* 2019; 237: 91–102. doi: 10.1016/j.apenergy.2019.01.015

[7] Shibata T, Sano T, Yano K, et al. Demonstration project of large-scale storage battery system at Minami-Hayakita substation – Evaluation of the 60MWh vanadium flow battery system performance –. *Grand Renewable Energy 2018*, 2018:283–286.

[8] Shibata T, Kumamoto T, Nagaoka Y, Kawase K, Yano K. Redox flow batteries for the stable supply of renewable energy.*SEI Technical review*, 2013:14–22.

[9] Guacaneme J, Garcerá G, Figueres E, Patrao I, González-Medina R. Dynamic modeling of a dual active bridge DC to DC converter with average current control and load-current feed-forward. *International Journal of Circuit Theory and Applications* 2015; 43(10): 1311–1332. doi: 10.1002/cta.2012

[10] Tseng KC, Kang JH, Tsai MH, Cheng CA. Analysis and implementation of a high step-up converter for fuel cell power-generation systems. *International Journal of Circuit Theory and Applications* 2016; 44(10): 1814–1827. doi: 10.1002/cta.2195

[11] Ramos Paja CA, Romero Nevado A, Giral Castillõn R, Martinez-Salamero L, Sanchez Saenz CI. Switching and linear power stages evaluation for PEM fuel cell emulation. *International Journal of Circuit Theory and Applications* 2011; 39(5): 475–499. doi: 10.1002/cta.651

[12] Mannari T, Okuda T, Hikihara T. Model for charging/discharging dynamics of cells in redox flow battery with transport delay. *Physica Scripta* 2019; 94(9): 095005. doi: 10.1088/1402-4896/ab1acd

[13] Shah AA, Tangirala R, Singh R, Wills RGA, Walsh FC. A Dynamic Unit Cell Model for the All-Vanadium Flow Battery. *Journal of The Electrochemical Society* 2011; 158(6): A671. doi: 10.1149/1.3561426

[14] Li Y, Skyllas-Kazacos M, Bao J. A dynamic plug flow reactor model for a vanadium redox flow battery cell. *Journal of Power Sources* 2016; 311: 57–67. doi: 10.1016/j.jpowsour.2016.02.018

[15] Yoshimoto K, Nanahara T, Koshimizu G. New Control Method for Regulating State-of- Charge of a Battery in Hybrid Wind Power/Battery Energy Storage System. In: IEEE; 2006: 1244–1251

[16] Teleke S, Baran M, Huang A, Bhattacharya S, Anderson L. Control Strategies for Battery Energy Storage for Wind Farm Dispatching. *IEEE Transactions on Energy Conversion* 2009; 24(3): 725–732. doi: 10.1109/TEC.2009.2016000

[17] Shibata Toshikazu , Kumamoto Takahiro , Nagaoka Yoshiyuki , Kawase Kazunori , Yano Keiji . Redox Flow Batteries for the Stable Supply of Renewable Energy. *SEI Technical Review* 2013; 76: 14–22

[18] Li MH, Funaki T, Hikihara T. A study of output terminal voltage modeling for redox flow battery based on charge and discharge experiments. In: ; 2007: 221–225

[19] Poullikkas A. Study of Electrode Reactions and Interfacial Properties. In: John Wiley & Sons, Ltd. 2006 (pp. 29–66)

[20] Akter MP, Li Y, Bao J, et al. Charging Control of Vanadium Redox Battery Based Energy Storage Systems with Variable Input Power. *2018 IEEE 27th International Symposium on Industrial Electronics (ISIE)* 2018: 489–494.

[21] Akter M, Li Y, Bao J, Skyllas-Kazacos M, Rahman M. Optimal Charging of Vanadium Redox Flow Battery with Time-Varying Input Power. *Batteries* 2019; 5(1): 20. doi: 10.3390/batteries5010020

[22] Bergveld Henk Jan and Kruijt WS, L NPH. Basic information on batteries. In: Dordrecht: Springer Netherlands. 2002 (pp. 31–53)

[23] Sukkar T, Skyllas-Kazacos M. Water transfer behaviour across cation exchange membranes in the vanadium redox battery. *Journal of Membrane Science* 2003; 222(1-2): 235–247. doi: 10.1016/S0376-7388(03)00309-0

[24] Li M, Hikihara T. A coupled dynamical model of redox flow battery based on chemical reaction, fluid flow, and electrical circuit. *IEICE Transactions on Fundamentals of Electronics, Communications and Computer Sciences* 2008; E91-A(7): 1741–1747. doi: 10.1093/ietfec/e91-a.7.1741

[25] Theodore L. The Conservation Laws. In: John Wiley & Sons, Ltd. 2012 (pp. 127–146)

[26] Virk GS. Runge Kutta method for delay-differential systems. *IEE Proceedings D - Control Theory and Applications* 1985; 132(3): 119–123. doi: 10.1049/ip-d.1985.0021

[27] Press WH, Teukolsky SA, Vetterling WT, Flannery BP. Integration of Ordinary Differential EquationsOrdinary Differential Equations. In: Cambridge University Press. 2002.

[28] Guarnieri M, Trovò A, Marini G, Sutto A, Alotto P. High current polarization tests on a 9 kW vanadium redox flow battery. *Journal of Power Sources* 2019; 431: 239–249. doi: 10.1016/j.jpowsour.2019.05.035